CrystEngComm

PAPER

View Article Online
View Journal | View Issue

Cite this: *CrystEngComm*, 2015, **17**, 3243

One-step synthesis of high-quality homogenous Te/Se alloy nanorods with various morphologies†

Shilin Fu, Kai Cai, Long Wu and Heyou Han*

Received 28th November 2014,
Accepted 9th March 2015

DOI: 10.1039/c4ce02352h

www.rsc.org/crystengcomm

A convenient method was developed for controllable synthesis of homogeneous trigonal Te/Se alloy nanorods (t-Te/Se ANRs) with diverse morphologies, aspect ratios and compositions at room temperature in aqueous solution. These alloy nanorods were formed by a self-seeding process. By varying the molar ratio of TeO_2 to H_2SeO_3 (x(Te : Se)) in the initial precursors, the morphology of t-Te/Se ANRs was transformed mainly *via* two paths: formation of tri-fold nanorods (TNRs) or single nanorods (SNRs). The nanostructures of TNRs were generated only by using x(Te : Se) ranging from 30 : 1 to 10 : 1, and SNRs were formed using x(Te : Se) ranging from 200 : 1 to 100 : 1 or 2 : 1 to 1 : 1. The microstructures, compositions, and growth mechanisms of these nanorods were also analyzed in detail.

Introduction

Tellurium (Te) and selenium (Se) are p-type semiconductors with a narrow band gap and high activity in hydration and oxidation reactions, due to these Te, Se and Te/Se alloys are utilized in the fields of gas sensing, thermoelectricity, photoconductivity and template method synthesis.[1–10] Te/Se alloys are composed of composite Te–Se atom-bonded helical chains, which are randomly united *via* van der Waals forces to form highly anisotropic crystal structures.[11–13] Particularly, nanodevices based on Te/Se alloys have many stimulating properties, such as electrical resistance and magnetoresistance, superior to pure Te and Se nanomaterials.[10,11,14,15] The morphologies of Te and Se nanostructures, just like Te or Se nanorods, have been extensively investigated in previous studies.[2,13,16–30] However, the study on t-Te/Se ANRs is still in its primitive stage in terms of morphology diversity, uniformity and synthesis method.[31–35] Currently, little information is available about the morphology of trigonal Te/Se alloy tri-fold nanorods (t-Te/Se ATNRs). For the sake of expanding the category of Te/Se alloy nanocrystals, recent research has been devoted to controllable synthesis of these homogeneous semiconductor nanocrystals.

Both trigonal tellurium (t-Te) and trigonal selenium (t-Se) belong to the hexagonal–trigonal crystal system, and are very identical to each other in the crystal form.[11,13] Pure tellurium dioxide and selenious acid can be easily crystallized together into hexagonal nanoplatelets because of the anisotropic and isomorphous characteristics of Te and Se.[11] The produced Te and Se atoms strongly tend to grow randomly along the *c*-axis of the crystal lattice to form nanorods through homogeneous nucleation and self-seeding process.[11,13] Te and Se have many similar chemical, physical and crystalline properties, but also have some differences in those aspects as well, which results in the growth of t-Te/Se ANRs different from either Te or Se nanostructures. For example, in a certain molar proportion range of Te and Se precursors the t-Te/Se ANRs turned out to be tri-rods.[31]

Herein, we demonstrate a facile one-pot solution approach to synthesize t-Te/Se ANRs of various morphologies with well-defined shapes, uniform sizes and large quantities. The growth mechanisms and microstructures of the t-Te/Se ANRs with various morphologies were also investigated in detail. This research provides a convenient route for controllable synthesis of homogeneous t-Te/Se ANRs with diverse morphologies, aspect ratios, compositions and lattice constants, which may hold promise for potential applications in the fields of photoconductivity and thermoelectricity.[2,28]

Experimental section

Materials

Tellurium dioxide (TeO_2, Aladdin, 99.99%), selenious acid (H_2SeO_3, Aladdin, 99.99%), sodium dodecyl sulfate (SDS, Aldrich, 99.99%) and hydrazine monohydrate ($N_2H_4{\cdot}H_2O$, Sinopharm, 85%, AR) were used as-purchased. 18 MΩ cm

State Key Laboratory of Agricultural Microbiology, College of Science, Huazhong Agricultural University, Wuhan 430070, PR China.
E-mail: hyhan@mail.hzau.edu.cn

† Electronic supplementary information (ESI) available: TEM image of amorphous Te/Se alloys obtained under reaction conditions: x(Te : Se) = 1 : 10 and growth time of 10 min. See DOI:10.1039/c4ce02352h

deionized water (E-Pure, Dubuque, IA) was used during the whole experimental process.

Synthesis of t-Te/Se ANRs

TeO_2 powder and H_2SeO_3 (aqueous solution, 0.2 M) were placed in glassware and mixed fully before the reaction began. The integral molar ratio of TeO_2 and H_2SeO_3 was 0.1 mmol, and the solution was supplemented with 10 mL of $N_2H_4{\cdot}H_2O$ in the reaction container under constant stirring and kept in a water bath at 33 °C for 30 min. The reaction was terminated by adding the as-prepared products into 50 mL of SDS solution (10 mM) to stabilize the products, followed by washing the unreacted mixtures and separation of SDS by centrifugation.

Characterization methods

High-resolution transmission electron microscopy (HRTEM) images and energy-dispersive X-ray spectroscopy (EDS) spectra were obtained with a JEOL JEM 2100F electron microscope operated at 200 KeV. The Raman spectra were obtained with a Raman spectrometer (Renishaw, UK) equipped with a confocal microscope (Leica, Germany) using an Ar laser (514.5 nm). The energy dispersive X-ray fluorescence (EDXRF) spectra were acquired by using an EAGLE III at 38 KeV for elemental analysis. Powder X-ray diffraction (XRD) data were collected using a Bruker D8 Advance diffractometer with Ni-filtered Cu Kα radiation (40 kV, 40 mA, λ = 0.15418 nm). The UV-visible (UV-vis) absorption spectra of the as-prepared t-Te/Se ANR suspensions were recorded using a UV-vis spectrophotometer (PerkinElmer, Lambda 25) over the spectral range of 200–900 nm.

Results and discussion

Fig. 1 shows that the Te and Se atoms can randomly form trigonal homogeneous crystals because of their identical hexagonal crystal structures; the hexagonal crystal structure consists of Te–Se bonded helical chains which form the highly anisotropic crystal structure of t-Te/Se ANRs.[11,13]

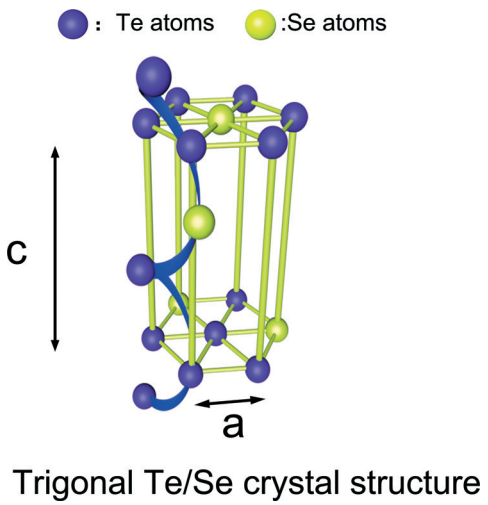

Fig. 1 The schematic of the trigonal Te/Se crystal structure.

The t-Te/Se ANRs were synthesized by reducing TeO_2 and H_2SeO_3 simultaneously in the presence of excess $N_2H_4{\cdot}H_2O$ in aqueous medium through the hydrothermal reaction:

$$xTeO_2 + yH_2SeO_3 + (x + y)N_2H_4 \rightarrow Te_xSe_y + (x + y)N_2 + (2x + 3y)H_2O$$

In a typical procedure, TeO_2 powder and an aqueous solution of H_2SeO_3 were mixed fully before $N_2H_4{\cdot}H_2O$ was added into the glassware to ensure the uniformity of the products. The reaction was processed in a water bath under constant stirring. The colour of the reaction solution changed rapidly even at low temperature from colourless to brown within 30 seconds, then turned dark brown and finally nearly black. This phenomenon was different from either pure TeO_2 which changed from colourless to purple and then to blue, or H_2SeO_3 which changed from colourless to red and then to opaque brick-red.[21,26] This change indicated that the t-Te/Se ANRs were produced at the initial moment, so the colour of the aqueous solution turned brown rather than violet or red at the initial moment of reaction.

Morphologies of t-Te/Se ANRs

The initial molar ratio of TeO_2 to H_2SeO_3 played a vital role in the nanostructures and aspect ratios of t-Te/Se ANRs. Fig. 2 illustrates that the TNRs were formed only when x(Te : Se) ranging from 30 : 1 to 10 : 1 were used (Fig. 2c and d), and that the morphology of the TNRs was actually three small hexagonal prisms that were combined, as depicted in Fig. 2II. However, once beyond these values, the t-Te/Se ANRs became SNRs (Fig. 2a, b, e and f). Fig. 2I and III show the schematics of the SNRs. All of the t-Te/Se ANRs have distinct shapes, monodisperse structures and uniform size.

When the values of x(Te : Se) were relatively high, such as 200 : 1 (Fig. 2a) and 100 : 1 (Fig. 2b), the morphologies of the t-Te/Se ANRs were SNRs. The inset in Fig. 2b shows the hexagonal cross section of a SNR which was highlighted by the red frame. The trigonal Te/Se alloy single nanorods (t-Te/Se ASNRs) tended to have a lower aspect ratio than pure Te nanorods, but a higher aspect ratio than amorphous Se.[21,26] Hence, compared to previous work, it can be concluded that the addition of a small proportion of Se to pure Te nanowires (Te NWs) reduced the length of the Te NWs.

It is worth noting that when x(Te : Se) = 30 : 1 to 10 : 1, the SNRs were converted into TNRs (Fig. 2c and d). The morphologies changed little from Fig. 2c to Fig. 2d. The insets in Fig. 2d show clear views of the vertical section and the cross section, with the left inset displaying the magnification of the vertical section view highlighted by the upper red frame, and the right inset illustrating the magnified TEM image of the cross-sectional view of a TNR marked by the lower red frame. Fig. 2II displays a 3-dimensional schematic showing

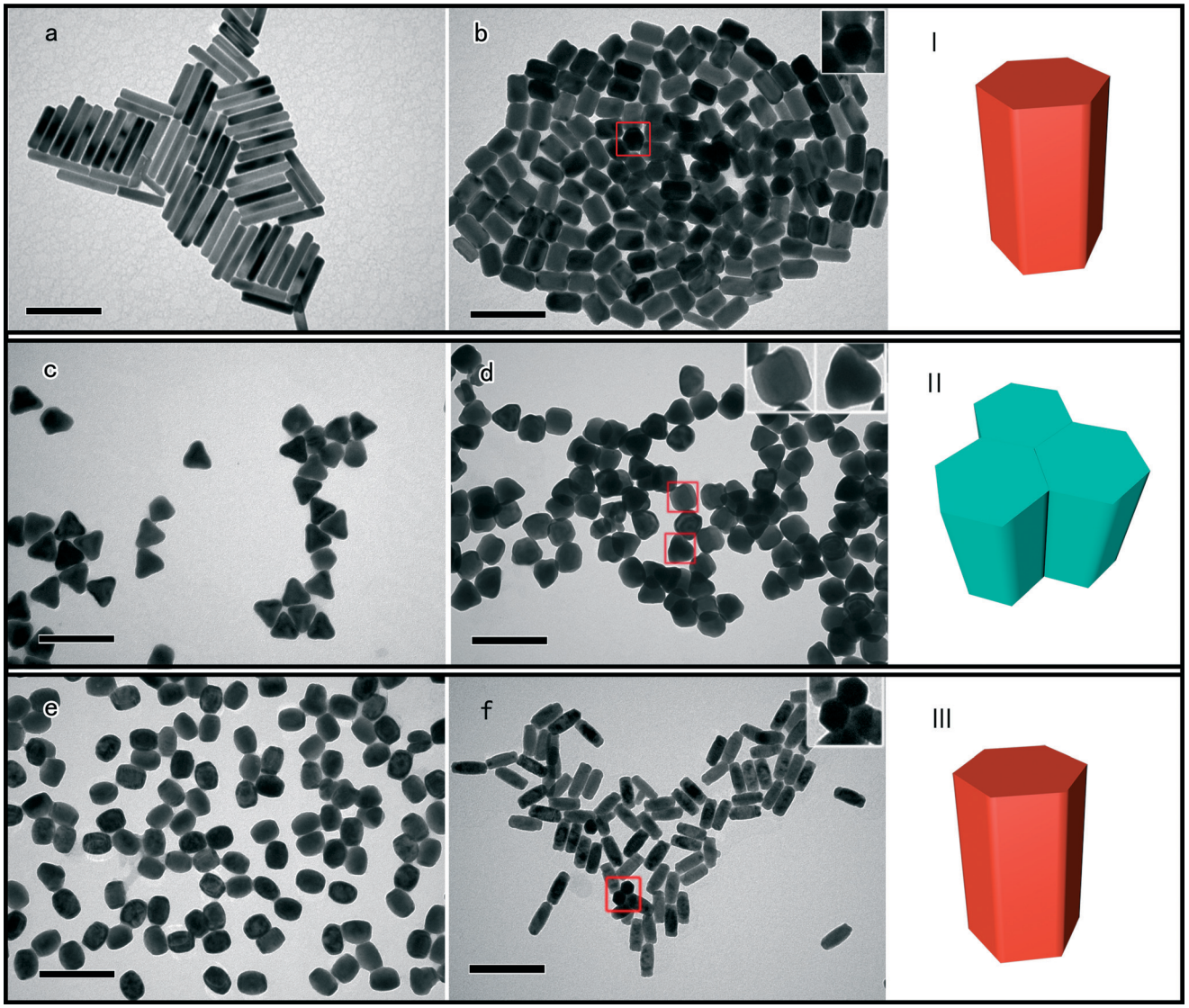

Fig. 2 TEM images of t-Te/Se ANRs generated with different values of *x*(Te : Se): (a) 200 : 1, (b) 100 : 1, (c) 30 : 1, (d) 10 : 1, (e) 2 : 1 and (f) 1 : 1. The insets in (b), (d) and (f) show the exact cross section morphologies of the nanorods. Image I represents (a) and (b), II (c) and (d), and III (e) and (f). The scale bars in the pictures represent 200 nm.

the exact tri-hexagonal shape of the TNRs. The t-Te/Se ATNRs could only be generated within a specific value range of *x*(Te : Se) which is probably due to the weaker crystalline nature of Se than that of Te. A higher proportion of Se resulted in the decrease in crystallization speed and further facilitated the separate nucleation.

With a further decrease in the value of *x*(Te : Se) to 2 : 1 and 1 : 1, the morphologies of t-Te/Se ANRs became SNRs again (Fig. 2e, f). Their shapes turned out to be a little shuttle-like, with the central section wider, and the aspect ratios became higher. This was probably because more Se facilitated both the amorphous and trigonal tendency of the Se element in the t-Te/Se ANRs, leading to expansion of the middle section and an increase in the length of the nanocrystals.[10] However, when *x*(Te : Se) dropped to 1 : 10 (Fig. S1, ESI†), we could only observe some spherical colloids at 10 min and nothing was detectable at 30 min, also probably due to the weaker crystalline nature of Se than that of Te. Therefore, with a higher proportion of Se in the Te/Se alloy, the amorphous nature dominated the crystallization process, leading to the formation of amorphous Te/Se (a-Te/Se) alloys with free energy higher than that of t-Te/Se ANRs, and as the redox reaction proceeded, the a-Te/Se alloys were converted into Te^{2+} and Se^{2+} by reduction of excess $N_2H_4{\cdot}H_2O$.[21]

Characterization

Fig. 3 shows the UV-vis spectra of the t-Te/Se ANRs fabricated using different molar ratios of TeO_2 to H_2SeO_3 ((a) 200 : 1, (b) 100 : 1, (c) 30 : 1, (d) 10 : 1, (e) 2 : 1 and (f) 1 : 1). The spectra show a red shift with the Te proportion rising and the Se proportion dropping until a *x*(Te : Se) value of 30 : 1. There was

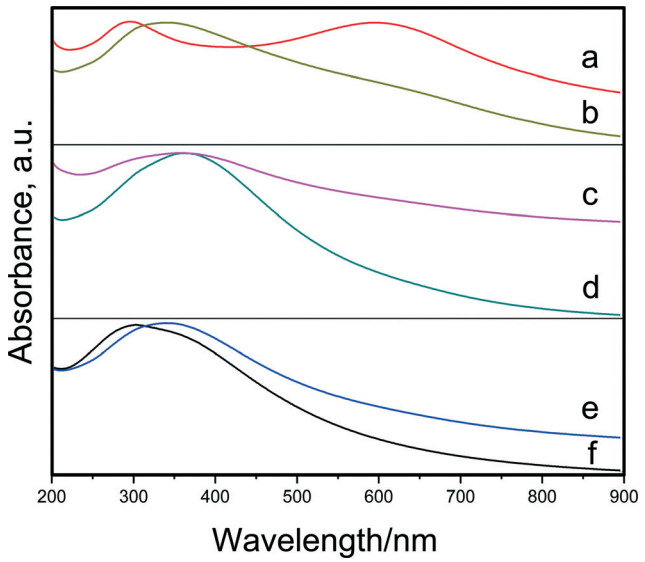

Fig. 3 UV-vis spectra of the t-Te/Se ANRs with *x*(Te : Se) values of (a) 200 : 1, (b) 100 : 1, (c) 30 : 1, (d) 10 : 1, (e) 2 : 1 and (f) 1 : 1.

little shift in the spectra between the ratios of 30 : 1 and 10 : 1. When the *x*(Te : Se) values decreased to 2 : 1 and 1 : 1, blue shifts occurred. These significant spectral shifts might be assigned to the variation in the length of the t-Te/Se ANRs from 180 nm to 70 nm (red shifts) and then to 130 nm (blue shifts), in which longer t-Te/Se ANRs led to lower values of the wavelength.

The microstructures of the t-Te/Se ANRs were further analyzed by HRTEM measurement (Fig. 4). The t-Te/Se ANRs with *x*(Te : Se) = 200 : 1, 15 : 1 and 1 : 1 are shown in Fig. 4a, c and e, respectively. The lattice fringes shown in Fig. 4b are 0.5882 nm, 0.4000 nm and 0.3333 nm which correspond to the (001), (100) and (101) planes of t-Te/Se ANRs. The lattice fringe spacings of t-Te and t-Se are listed as follows: Te_{001} = 0.5926 nm, Te_{100} = 0.3856 nm and Te_{101} = 0.3233 nm (JCPDF no. 36-1452); Se_{001} = 0.4950 nm, Se_{100} = 0.3780 nm and Se_{101} = 0.3005 nm (JCPDF no. 06-0362). Fig. 4b shows that the t-Te/Se ANRs grew along the [001] direction. The HRTEM image in Fig. 4d was taken perpendicularly to the (001) plane of a t-Te/Se ATNR, and all the lattice spacings were 0.3878 nm which could be indexed to the $(10\bar{1}0)$, $(01\bar{1}0)$ and $(1\bar{1}00)$ planes of t-Te/Se ATNRs, indicating that the t-Te/Se ATNRs also grew along the [001] direction. The lattice distances of the (110) and (003) planes calculated from the electron diffraction diagram were 0.2260 nm and 0.1934 nm. The lattice fringe spacings in Fig. 4f were 0.5670 nm, 0.3829 nm and 0.3276 nm, which correspond to the (001), (100) and (101) planes, respectively. Therefore, the nanorods with *x*(Te : Se) = 1 : 1 tended to grow along the [001] direction as illustrated in Fig. 4f. The insets in Fig. 4b and f are Fast Fourier Transformation (FFT) images and the inset in Fig. 4d is the electron diffraction pattern.

The real compositions of the t-Te/Se ANRs were clarified by EDXRF (Fig. 5a–c). The initial *x*(Te : Se) values of the precursors were (a) 200 : 1, (b) 15 : 1 and (c) 1 : 1, which correspond to Fig. 4a, c and e. The peaks of Se increased obviously with

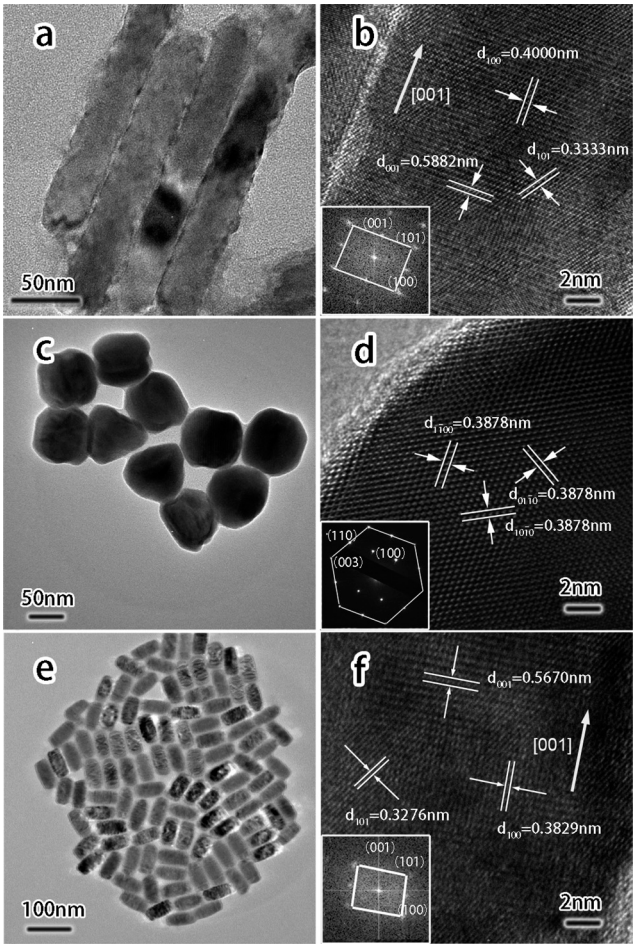

Fig. 4 t-Te/Se ANRs with *x*(Te : Se) = (a) 200 : 1, (c) 15 : 1 and (e) 1 : 1. (b). (d) and (f) are the HRTEM images of the t-Te/Se ANRs in (a), (c) and (e). The insets in (b) and (f) indicate the Fast Fourier Transformation (FFT) images and (d) is the electron diffraction diagram.

decreasing *x*(Te : Se), and the real values of Te : Se for the three groups of t-Te/Se ANRs were (a) 194 : 1, (b) 12 : 1 and (c) 4.6 : 1. The 'S' peaks in the spectra correspond to the sulphur element in SDS ($C_{12}H_{25}SO_4Na$) adhered to the t-Te/Se ANRs.

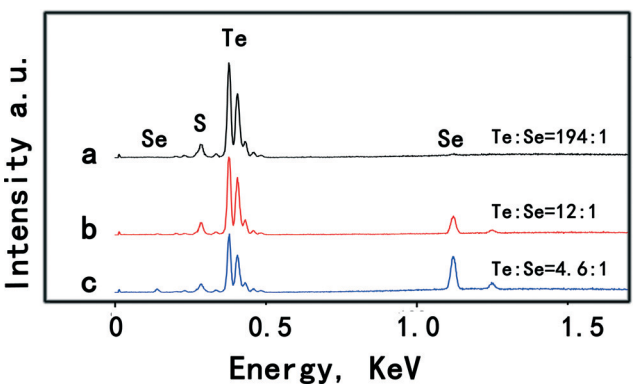

Fig. 5 EDXRF spectra (a)–(c) reveal the actual atom ratios of Te to Se in the t-Te/Se ANRs corresponding to Fig. 4(a), (c) and (e), in which the *x*(Te : Se) values are 200 : 1, 15 : 1 and 1 : 1, respectively.

The actual Se content of the nanorods was identical to that when x(Te : Se) = 200 : 1 and 15 : 1, but it obviously increased when x(Te : Se) = 1 : 1. This dramatic increase in Se content might be a result of the weaker crystalline nature of Se than that of Te, so the nanorods tended to have more Te to ensure the high crystallinity of the t-Te/Se ANRs.[31]

The lattice constants of the t-Te/Se ANRs were analyzed by XRD (Fig. 6a–c). Alterations in the x(Te : Se) also led to ultimate changes in the lattice constants of the t-Te/Se ANRs.

Fig. 6a–c show the XRD patterns of the nanorods corresponding to those in Fig. 4a, c and e, in which x(Te : Se) = 200 : 1, 15 : 1 and 1 : 1, respectively. These patterns were similar to those of pure Te (blue line, JCPDF no. 36-1452) and Se (red line, JCPDF no. 06-0362), indicating that the nanorods were well crystallized trigonal crystals. The (101) peaks of the t-Te/Se ANRs were also found to be between the (101) peaks of pure t-Te and t-Se. The lattice constants were calculated and the results were found to be between those of pure t-Te (a = 0.4458 nm, c = 0.5927 nm) and pure t-Se (a = 0.4366 nm, c = 0.4954 nm), which were (a) a = 0.4516 nm, c = 0.5895 nm, (b) a = 0.4454 nm, c = 0.5874 nm, and (c) a = 0.4466 nm, c = 0.5773 nm. With a higher percentage of Se, the 2-theta degrees of the (101) peaks became closer to those of pure t-Se. In addition, the t-Te/Se ANRs fabricated using a lower proportion of Te and a higher proportion of Se in the ratio of Te to Se showed a weaker intensity of XRD peaks, which can be seen obviously from the (101) peaks presented in Fig. 6a–c (Fig. 6, inset). That is probably because the intensity of the XRD peaks of pure t-Se is weaker than that of pure t-Te.

The Raman spectra of the t-Te/Se ANRs were studied. The x(Te : Se) values of the t-Te/Se ANRs in Fig. 7a–c were 200 : 1, 15 : 1 and 1 : 1, respectively. The peaks in Fig. 7a are 117.52, 135.37 and 260.02 cm^{-1}, the peaks in Fig. 7b are 119.19, 136.91, 163.41 and 221.45 cm^{-1} and the peaks in Fig. 7c are 127.57, 139.82, 170.95 and 260.17 cm^{-1}. These results were similar to those of pure t-Te but shifted to high frequency.[36–38] This may be attributed to the Se added into the nanorods because pure t-Se had higher-frequency Raman spectra.[39] Also, different crystallinity between the materials can also lead to these results.[38]

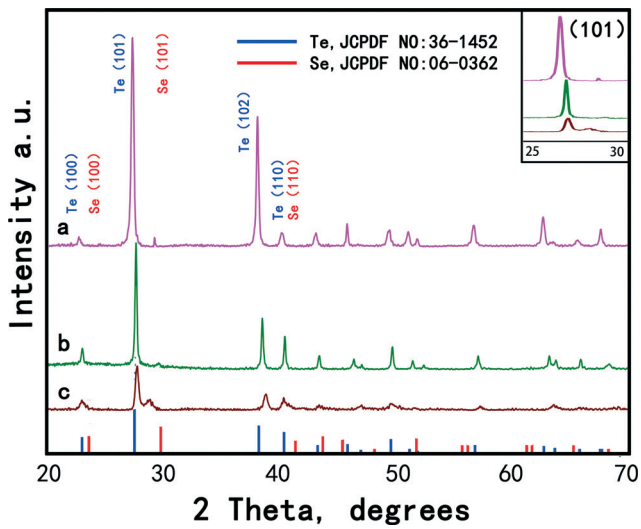

Fig. 6 XRD patterns of the t-Te/Se ANRs with three different values of x(Te : Se): (a) 200 : 1, (b) 15 : 1 and (c) 1 : 1. The peaks indicate that the t-Te/Se ANRs are single crystallites and belong to the trigonal phase. The inset magnifies the (101) peaks of the three t-Te/Se ANRs.

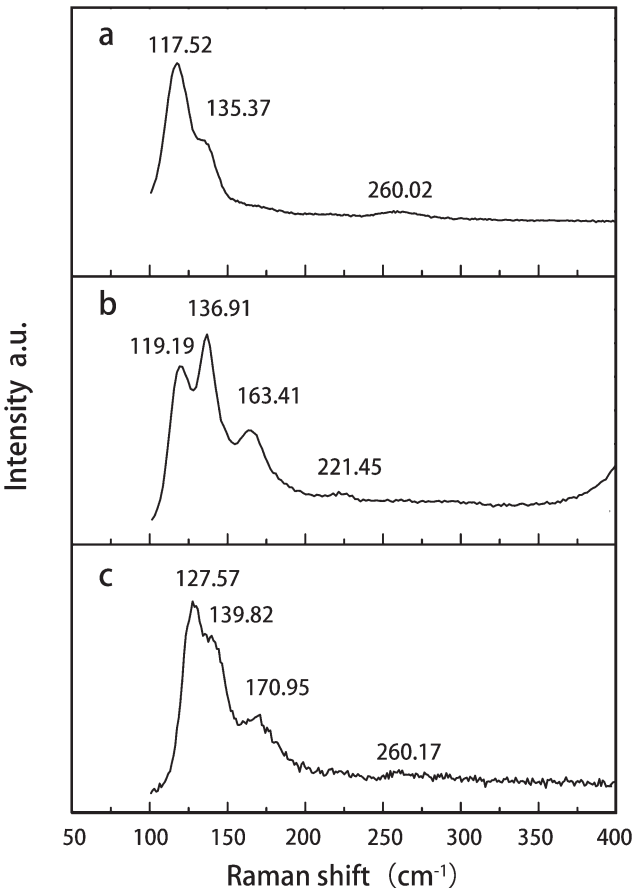

Fig. 7 Raman scattering spectra of the t-Te/Se ANRs. The x(Te : Se) values of the t-Te/Se ANRs are (a) 200 : 1, (b) 15 : 1 and (c) 1 : 1.

Growth mechanism of t-Te/Se ANRs

The self-seeding nucleation and growth process were studied and the morphology transformation process was illustrated by TEM images. Fig. 8 shows the TEM images of the morphology evolution of t-Te/Se ATNRs with x(Te : Se) = 10 : 1 at time periods of (a) 10 min, (b) 20 min, (c) 60 min and (d) 240 min as well as the schematic of the four-step shape transformation (Fig. 8e). The growth mechanism of the t-Te/Se ATNRs followed that of tri-tip t-Te.[12] The t-Te/Se ATNRs grew first as small hexagonal prisms (Fig. 8a, inset and e(I)) within a period of 10 min, and then the Te and Se atoms selectively deposited on 3 surfaces of the initial hexagonal prism to form 3 new hexagonal prisms (Fig. 8b and e(II)) within a period of 20 min. With further reduction and growth at 60 min, the 3 new hexagonal prisms became bigger and their

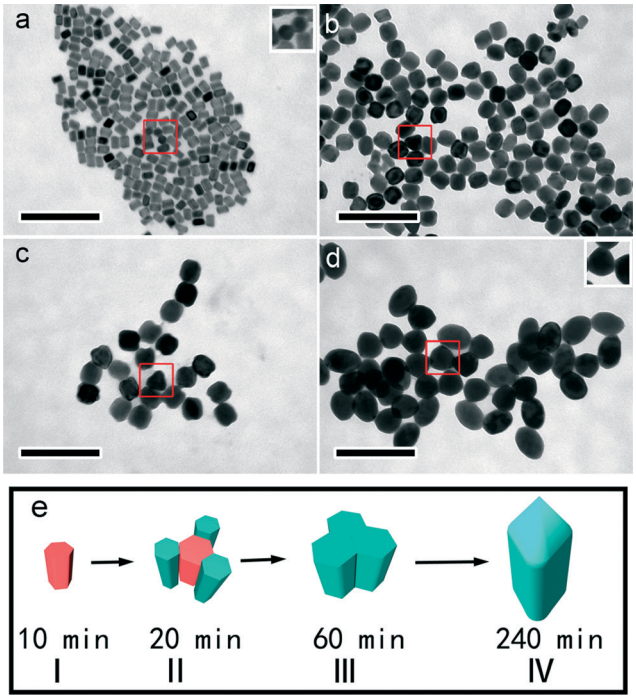

Fig. 8 TEM images showing the morphologies of the t-Te/Se ATNRs with *x*(Te : Se) = 10 : 1 at time periods of (a) 10 min, (b) 20 min, (c) 60 min and (d) 240 min. Red frames indicate the cross section of the nanorods. Insets in (a) and (d) show the cross section of the t-Te/Se ATNRs in (a) and (d). (e) The schematic of the t-Te/Se ATNR evolution process. All of the scale bars in the pictures represent 200 nm.

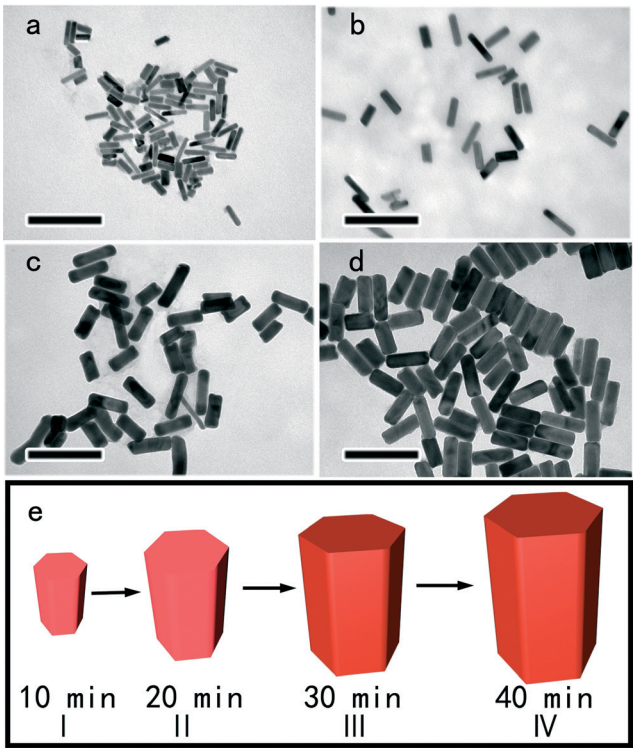

Fig. 9 TEM images of t-Te/Se ASNR growth with *x*(Te : Se) = 125 : 1 at time periods of (a) 10 min, (b) 20 min, (c) 30 min and (d) 40 min. The SNRs just grew bigger as the reaction proceeded. (e) The schematic of t-Te/Se ASNR evolution.

central gap was filled up (Fig. 8c and e(III)). Finally, the edges of the ATNRs became vaguer and the nanoparticles formed an ellipsoid shape at 240 min (Fig. 8d and e(IV)). The inset in Fig. 7d is the cross section of the t-Te/Se ATNRs supporting this mechanism.

Fig. 9 shows the TEM images of t-Te/Se ASNR growth with *x*(Te : Se) = 125 : 1 at time periods of (a) 10 min, (b) 20 min, (c) 30 min and (d) 40 min, within which the SNRs grew from 70 ± 10 nm (Fig. 9a) to 140 ± 15 nm (Fig. 9d) in length, and from 10 ± 3 nm to 40 ± 5 nm in diameter, indicating that the SNRs just became bigger as the redox reaction proceeded. The transformation process was similar to the growth process of pure t-Te.[21]

Fig. 10 summarizes the two paths for the growth of t-Te/Se ANRs. Route 1 shows the general process for the growth of t-Te/Se ASNRs in which Te and Se atoms initially combined to form a hexagonal nucleus (seed) (Fig. 10I), and the Te/Se alloys only grew longer and wider (Fig. 10II and III) as the reaction progressed. Route 2 demonstrates the growth process of t-Te/Se ATNRs. The difference of Route 2 is that there is a separate nucleation process (Fig. 10IV) after the initial seeding process; the Te and Se atoms selectively deposited along the edge of the seed which brought about the shape of t-Te/Se ANRs as TNRs. As the reaction continued, the t-Te/Se ANRs in Fig. 10II and IV grew bigger into the t-Te/Se ANRs in Fig. 10III and V, respectively. The TNR phenomenon has been reported for pure Te NWs in a water and ethylene glycol mixture at high temperature or pressure, but little information is available about the TNRs of Te/Se alloys.[12,40,41]

The evolution mechanism was as follows: the Te and Se atoms were formed as Te–Se bonded helical chains,[11] these disorganized chains aggregated as amorphous Te/Se (a-Te/Se) at the initial moment, then the a-Te/Se (disorganized chains) transformed into trigonal Te/Se (organized chains) because of Rayleigh instability.[13] Fig. S2 (ESI†) showed the EDS

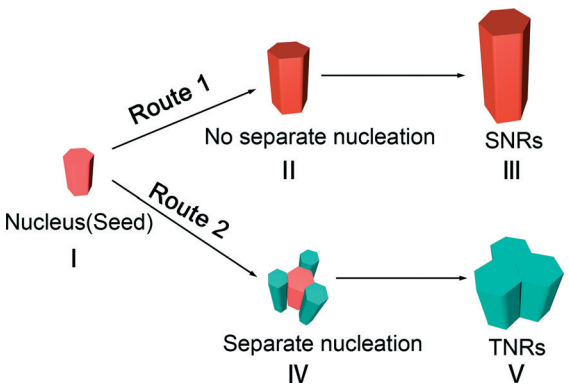

Fig. 10 Mechanism model for the two possible growth paths. Route 1 shows that the t-Te/Se ANRs grow directly from the initial hexagonal nuclear prisms (seeds) (I) into t-Te/Se ASNRs (III) without separate nucleation. Route 2 indicates that a separate nucleation process leads to transformation of the seeds into t-Te/Se ATNRs (IV). (II) and (IV) grow bigger into (III) and (V), respectively, as the reaction proceeds.

spectra of Fig. 7a and 8 and that indicated the real Te : Se values were 13 : 1 and 124 : 1, respectively, which means the seeds were Te/Se alloys.

This phenomenon may be attributed to the difference in both chemical kinetics and crystal kinetics. H_2SeO_3 can be more easily reduced than TeO_2, suggesting that H_2SeO_3 has higher reduction potential than TeO_2.[26] Additionally, Te is a metalloid with a more obvious crystalline nature than Se, which is a non-metal with an amorphous nature.[31] When Te and Se began to form homogeneous nanorods, their morphologies were influenced by the competition between the crystalline tendency of Te to grow into trigonal Te and the amorphous tendency of Se to grow into amorphous Se, suggesting that the morphology of t-Te/Se ANRs was sensitive to the original value of x(Te : Se). Therefore, when x(Te : Se) = 200 : 1 and 100 : 1, the trigonal Te nature dominated the morphology, which was similar to that of pure t-Te.[11,21] When x(Te : Se) = 2 : 1 and 1 : 1, the trigonal Se nature played the defining role in the morphology, which was identical to that of pure t-Se.[13] Only when the x(Te : Se) ranged from 30 : 1 to 10 : 1 could the t-Te/Se ANRs grow into TNRs under the mutual effects of the chemical and crystal properties of Te and Se.

Conclusions

We have developed a practical protocol for controllable generation of t-Te/Se ANRs with various morphologies, which changed from long and thin SNRs to TNRs and back to shuttle-like SNRs, by varying the reaction conditions. The lattice constants and compositions of the nanorods also varied with changes in the initial molar ratio of TeO_2 to H_2SeO_3. All the t-Te/Se ANRs possess distinct morphological characteristics in terms of uniformity and monodispersity. These high-quality nanomaterials remain stable in water for months.

As the compositions, morphologies and lattice constants can be well designed by tuning the parameters for the reaction, these novel high-quality nanostructures may have potential applications in thermoelectricity and photoconductivity and can also be used as sacrificial templates for synthesis of complex noble metal nanostructures like Au nanoframes.[1,42,43]

Acknowledgements

We gratefully acknowledge financial support from the National Natural Science Foundation of China (21375043, 21175051).

Notes and references

1 K. Cai, Z. Lv, K. Chen, L. Huang, J. Wang, F. Shao, Y. Wang and H. Han, *Chem. Commun.*, 2013, **49**, 6024–6026.
2 G. Zhang, H. Fang, H. Yang, L. A. Jauregui, Y. P. Chen and Y. Wu, *Nano Lett.*, 2012, **12**, 3627–3633.
3 H. H. Li, P. Zhang, C. L. Liang, J. Yang, M. Zhou, X. H. Lu and G. A. Hope, *Cryst. Res. Technol.*, 2012, **47**, 1069–1074.
4 W. S. Wang, J. Goebl, L. He, S. Aloni, Y. X. Hu, L. Zhen and Y. D. Yin, *J. Am. Chem. Soc.*, 2010, **132**, 17316–17324.
5 F. K. Butt, M. Mirza, C. Cao, F. Idrees, M. Tahir, M. Safdar, Z. Ali, M. Tanveer and I. Aslam, *CrystEngComm*, 2014, **16**, 3470–3473.
6 N. P. Dasgupta, J. Sun, C. Liu, S. Brittman, S. C. Andrews, J. Lim, H. Gao, R. Yan and P. Yang, *Adv. Mater.*, 2014, **26**, 2137–2184.
7 Z. Wang, L. Wang, J. Huang, H. Wang, L. Pan and X. Wei, *J. Mater. Chem.*, 2010, **20**, 2457.
8 H. Xu, G. Chen, R. Jin, D. Chen, Y. Wang, J. Pei, Y. Zhang, C. Yan and Z. Qiu, *CrystEngComm*, 2014, **16**, 3965–3970.
9 L. D. Zhao, S. H. Lo, Y. Zhang, H. Sun, G. Tan, C. Uher, C. Wolverton, V. P. Dravid and M. G. Kanatzidis, *Nature*, 2014, **508**, 373–377.
10 B. Sadtler, S. P. Burgos, N. A. Batara, J. A. Beardslee, H. A. Atwater and N. S. Lewis, *Proc. Natl. Acad. Sci. U. S. A.*, 2013, **110**, 19707–19712.
11 B. Mayers, B. Gates, Y. Yin and Y. Xia, *Adv. Mater.*, 2001, **13**, 1380–1384.
12 B. Mayers and Y. Xia, *J. Mater. Chem.*, 2002, **12**, 1875–1881.
13 B. Gates, B. Mayers, B. Cattle and Y. N. Xia, *Adv. Funct. Mater.*, 2002, **12**, 219–227.
14 Z.-H. Lin, P. Roy, Z.-Y. Shih, C.-M. Ou and H.-T. Chang, *ChemPlusChem*, 2013, **78**, 302–309.
15 K. Sridharan, M. S. Ollakkan, R. Philip and T. J. Park, *Carbon*, 2013, **63**, 263–273.
16 Z. Li, S. Zheng, Y. Zhang, R. Teng, T. Huang, C. Chen and G. Lu, *J. Mater. Chem. A*, 2013, **1**, 15046.
17 Q. Wang, M. Safdar, X. Zhan and J. He, *CrystEngComm*, 2013, **15**, 8475–8482.
18 J. Pei, G. Chen, D. Jia, R. Jin, J. Sun and Y. Yu, *CrystEngComm*, 2013, **15**, 241–244.
19 C. Chen, Y. Kang, Z. Huo, Z. Zhu, W. Huang, H. L. Xin, J. D. Snyder, D. Li, J. A. Herron, M. Mavrikakis, M. Chi, K. L. More, Y. Li, N. M. Markovic, G. A. Somorjai, P. Yang and V. R. Stamenkovic, *Science*, 2014, **343**, 1339–1343.
20 H. Zhu, J. Luo, H. Zhang, J. Liang, G. Rao, J. Li, G. Liu and Z. Du, *CrystEngComm*, 2012, **14**, 251–255.
21 Z.-H. Lin, Z. Yang and H.-T. Chang, *Cryst. Growth Des.*, 2008, **8**, 351–357.
22 C. J. Hawley, B. R. Beatty, G. Chen and J. E. Spanier, *Cryst. Growth Des.*, 2012, **12**, 2789–2793.
23 B. Zhang, W. Hou, X. Ye, S. Fu and Y. Xie, *Adv. Funct. Mater.*, 2007, **17**, 486–492.
24 H. S. Qian, S. H. Yu, J. Y. Gong, L. B. Luo and L. F. Fei, *Langmuir*, 2006, **22**, 3830–3835.
25 J. Zhang, S.-Y. Zhang and H.-Y. Chen, *Chem. Lett.*, 2004, **33**, 1054–1055.
26 U. Y. Jeong and Y. N. Xia, *Adv. Mater.*, 2005, **17**, 102–106.
27 X. M. Li, Y. Li, S. Q. Li, W. W. Zhou, H. B. Chu, W. Chen, I. L. Li and Z. K. Tang, *Cryst. Growth Des.*, 2005, **5**, 911–916.
28 J.-W. Liu, J.-H. Zhu, C.-L. Zhang, H.-W. Liang and S.-H. Yu, *J. Am. Chem. Soc.*, 2010, **132**, 8945–8952.
29 Q. Wang, M. Safdar, Z. Wang and J. He, *Adv. Mater.*, 2013, **25**, 3915–3921.

30 R. M. Ireland, L. Zhang, P. Gopalan and H. E. Katz, *Adv. Mater.*, 2013, **25**, 4358–4364.
31 G. Kaur and M. S. Bakshi, *J. Phys. Chem. C*, 2010, **114**, 143–154.
32 D.-H. Qin, H. Tao and Y. Cao, *Chin. J. Chem. Phys.*, 2007, **20**, 670–674.
33 B. Zhou and J.-J. Zhu, *Nanotechnology*, 2006, **17**, 1763–1769.
34 T. P. Vinod, M. Park, S. H. Kim and J. Kim, *Langmuir*, 2010, **26**, 9195–9197.
35 H. Tao, X. Shan, D. Yu, H. Liu, D. Qin and Y. Cao, *Nanoscale Res. Lett.*, 2009, **4**, 963–970.
36 S. Wang, K. Zhang, H. Zhou, W. Guan, D. Ma, J. Lin, L. Zhang, S. Huang and J. Wang, *CrystEngComm*, 2010, **12**, 3852–3857.
37 J.-W. Liu, F. Chen, M. Zhang, H. Qi, C.-L. Zhang and S.-H. Yu, *Langmuir*, 2010, **26**, 11372–11377.
38 J. M. Song, Y. Z. Lin, Y. J. Zhan, Y. C. Tian, G. Liu and S. H. Yu, *Cryst. Growth Des.*, 2008, **8**, 1902–1908.
39 L. Liu, Q. Peng and Y. Li, *Nano Res.*, 2008, **1**, 403–411.
40 S. Wang, W. Guan, D. Ma, X. Chen, L. Wan, S. Huang and J. Wang, *CrystEngComm*, 2010, **12**, 166–171.
41 L. Yang, Z.-G. Chen, G. Han, L. Cheng, H. Xu and J. Zou, *Cryst. Growth Des.*, 2013, **13**, 4796–4802.
42 M. McEachran, D. Keogh, B. Pietrobon, N. Cathcart, I. Gourevich, N. Coombs and V. Kitaev, *J. Am. Chem. Soc.*, 2011, **133**, 8066–8069.
43 N. R. Sieb, N. C. Wu, E. Majidi, R. Kukreja, N. R. Branda and B. D. Gates, *ACS Nano*, 2009, **3**, 1365–1372.

